34th Annual International Conference of the IEEE EMBS
San Diego, California USA, 28 August - 1 September, 2012

Improving active contour methods for tracking endothelial cells by the removal of low-confidence edge segments

Alireza Nejati, Charles P. Unsworth, *Member IEEE*, Euan S. Graham

***Abstract*— Previously we developed an active contour method for segmenting and tracking cells in phase-contrast microscopy images. Our method is capable of fine-grained segmentation on noisy image sequences. In this paper, we improve the active contour segmentation model to provide better accuracy, by selectively identifying areas of the contour with low confidence and removing them. The method is applied to HMEC-1 cells (human microvascular endothelial cells). The segmentation provided by the method is quantitavely compared with manually-drawn contours, showing close fit and capability to 'lock' on to cell boundaries for hundreds of frames.**

I. Introduction

Tracking biological cells is of importance in the biological sciences. Information obtained from tracking migrating cells in vitro (from e.g. scratch wounds [1]) can be used to study cell-cell interactions [2], cell division [3], differentiation [4], and identify cell necrosis and apoptosis (as these processes are marked by specific changes in morphology [5]).

Active contours [6] are a method of image segmentation that are used widely in the biological sciences, such as analysis of MRI images [7] and tracking cells [8][9]. In addition, recent work has been able to apply active contour techniques to very low-contrast images [10]. The active contour method is as follows: An initial boundary (the contour) is drawn around an object. The boundary is then deformed according to internal and external energy functionals to find a better fit around the object. A boundary for an object in one frame may be used as the starting point for its boundary in the next.

In the active contour variant given in this paper, only external energy is used. The contour is represented as a piecewise-linear curve, and it is subdivided to better fit into protrusions. Our method finds a globally optimal curve and has no internal energy.

II. Active contour method

Let the contour be represented as $\hat{p}(s) = (x(s), y(s))$, where s ranges from 0 to 1. Define the energy of the curve as:

$$E_X(\hat{p}) = -\left|\frac{1}{L}\int_0^1 \frac{1}{\|\mathbf{N}(s)\|}\mathbf{N}(s).\mathbf{G}(\hat{p}(s))ds\right| \quad (1)$$

A. Nejati is a PhD student in the Department of Engineering Science, University of Auckland, Auckland 1010, New Zealand. (phone: +64-9-373-7599 ext 87490; fax: +64-9-373-7468; email: alireza.n.j@gmail.com)

C. P. Unsworth is a Senior Lecturer in the Department of Engineering Science, The University of Auckland, Auckland 1010, New Zealand. email: c.unsworth@auckland.ac.nz

E. S. Graham is with the Department of Pharmacology & Centre for Brain Research, The University of Auckland, New Zealand

Where L is the total length of the curve, $\mathbf{G}$ is the underlying gradient field of the image (computed using a Sobel filter) and $\mathbf{N}$ is the normal vector of the curve. We calculate the gradient using the Sobel filter, due to its attractive properties of computational simplicity and locality.

In the rest of this paper, we assume our contour is piecewise-linear i.e. it is defined by a set of points $\hat{p}_i$ $(1 < i < n)$ that are connected together in sequence.

At each frame, we may extrude the vertices of the contour to better fit the image at the next frame (see Fig. 2). Instead of extruding in every possible direction, we only allow the vertex to be extruded normal to the curve. This greatly reduces the number of possible extrusions that need to be considered. This is also in line with cell dynamics in which membrane extrusion happens locally. The normal is calculated in a 'multi-scale' way so as to minimize the influence of small-scale noise on the extrusion. In detail, this is done by convolving the tangent vectors of the neighbors of each point with a gaussian with standard deviation proportional to the extrusion level. Consider, for example, a point $\hat{p}_i$ on the curve. The tangent vector at that point, for an extrusion level x, is given by:

$$\mathbf{T}_i = \sum_{j=i-M}^{i+M} e^{-c_{ij}^2/2x^2}(\hat{p}_i - \hat{p}_j) \quad (2)$$

Where M is some number chosen to be large enough so that the exponential decays to zero and the contour is assumed to 'wrap around' i.e. $\hat{p}_i = \hat{p}_{i+n}$ where n is the number of points on the contour. In addition, c_{ij} is the cumulative distance from $\hat{p}_i$ to $\hat{p}_j$:

$$c_{ij} = \sum_{k=i}^{j} \|\hat{p}_i - \hat{p}_j\| \quad (3)$$

The normal, then, is simply chosen to be the unit vector perpendicular to $\mathbf{T}_i$.

As mentioned previously, at each iteration we may extrude each pixel by an independent amount. We refer to a vector of extrusions levels, one for each vertex, as an *extrusion*. Note that we fix a limit to how far a vertex can be extruded. For the purposes of this paper, this limit has been set to 16 pixels.

One issue with the global minimization scheme is that since the number of vertices on the contour does not change it sometimes becomes problematic for the contour to fit into protrusions. To overcome this problem we used an iterative refinement scheme where a curve fitting step is performed, edges that have become stretched are subdivided,

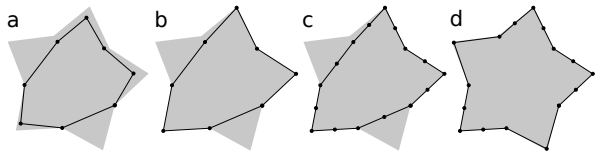

Fig. 1. Iterative refinement. a) Initial contour. b) Fit to image boundary. Due to roughness of contour, it is impossible to perfectly match the boundary. c) Refinement of boundary. d) New fit using refined boundary.

then another step is performed. This is done until the size of the subdivided segments gets down to the order of the size of the pixels, at which point further subdivision is not likely to yield improvments (see figure 1).

Given these definitions, our active contour method is as follows:

1) Manually draw contour r^0 for first frame.
2) Simplify the contour.
3) For contour r^k, obtain r^{k+1} by finding the extrusion that minimizes the global energy E_X of the curve.
4) Subdivide the curve and repeat steps 2 and 3 unless the length of each segment goes below one pixel.
5) Advance to the next frame and repeat steps 2-4 until the end of the data series.

Simplification (step 2) is only done to ease the computational load, and may be omitted. The simplification is performed heuristically by removing vertices until no edge is of length larger than a given threshold (chosen arbitrarily as 8 pixels for the purposes of this paper). Vertices are not removed if they are on sharp corner (less than or equal to 45 degrees). Step 3 is performed using the Bellman-Ford algorithm. Since the exact global minimum is always found, the details of the minimization algorithm are not relevant to the results presented in this paper.

A. Improvements

The iterative subdivision scheme (steps 3-4 in the algorithm) allows for effective protrusion of the contour into rapidly-protruding areas of the cell. However, it is less effective at fitting into retracting protrusions. This can be seen in Fig. 6 and is depicted schematically in Fig. 4. In addition, the initial version of our method suffered from self-intersections that had to be automatically-removed at each step (see Figs. 2 and 5). Both of these problems were solved by simply including a procedure that removes low-confidence areas of the contour (see Fig. 4), where confidence is defined as simply the local edge energy according to equation 1. We arbitrarily chose 5% of the maximum possible edge energy as a cutoff level below which edges should be removed. We term this procedure *low-confidence removal*. We found that under this scheme, the number of self-intersections were reduced (as an example, see Fig. 5). This is because the lower rate of self-intersection testing (once per frame instead of once per step) allows minor perturbations in the curve that cause self-intersections the chance to be corrected before clipping takes place.

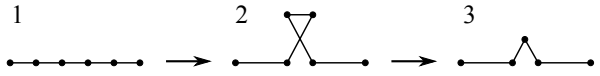

Fig. 2. Intersection removal. After fitting, some parts of the contour may develop self-intersections. In the first iteration of our method, we solve this by cutting out the intersection loops (3). In our improved method, we do this by removing areas of low confidence.

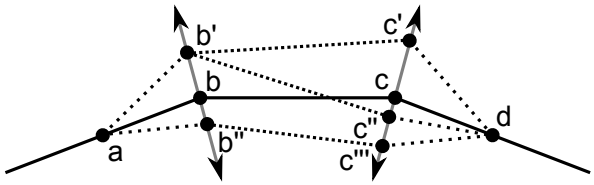

Fig. 3. Extrusion at each frame. The original contour is the solid line, and a new contour may be produced by extruding, for example, points b and c by any amount.

III. Materials and Methods

The HMEC-1 cells were obtained from ATCC under licence from the CDC (Centre for Disease Control). Cells were cultured in MCDB-131 media (Invitrogen) supplemented with 10% fetal bovine serum (FBS), l-glutamine (10mmol/L), penicillin/ streptomycin. Culturing took place in a CO2/O2 incubator at 37C. Once cells reached confluence they were harvested by trypsinisation. Cells (low passage 612) were seeded into 30mm Petri dishes (Nunc) containing with silicon inserts (ibidi). Cells were seeded at a very low density of approximately 5000 cells/cm2. Time lapse experiments were conducted with a Nikon Biostation™ IM. Cells and dishes were allowed to equilibrate for 20-30 minutes in the Biostation chamber prior to imaging to allow the temperature/humidity to equilibrate and remove any condensation. During this time, regions of interest were determined and programmed using the Biostation IM software. Data were collected as original Biostation .NES files and also converted to AVI movies for visualisation.The time-lapse series was constructed by taking a single image of each region of interest every 2 minutes. Data analysis was conducted on the original time-lapse stills extracted from the NES files. Our own custom software was used for producing outlined and tiled images. Sample cell movements and the outlines produced by our software can be seen in Fig. 7.

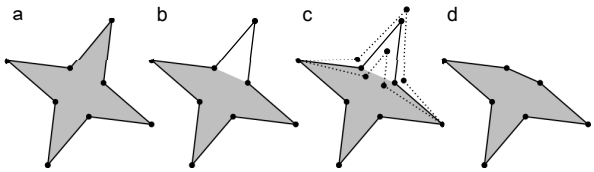

Fig. 4. Confidence-based contour adjustment. The contour (black dots connected by solid line) has been fit to the image (a). At the next frame, the cell retracts a previously-extended protrusion (b). Extrusion-based fitting cannot find an optimal fit to the image, because the angle of the new contour is roughly orthogonal to the original contour (c). However, if we remove the parts of the contour that have low confidence, a good fit can be obtained (d).

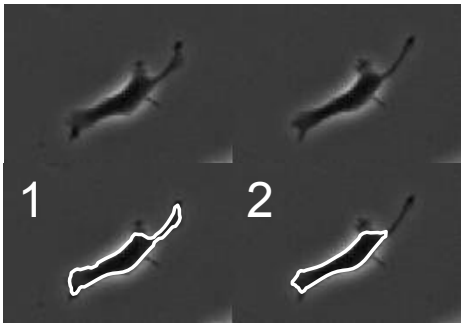

Fig. 5. Removal of self-intersections leads to the occasional clipping of narrow cell protrusions (bottom). Numbers indicate frame number; frame 1 is the first automatically-found frame (this is the same in all other figures). Frame 2 is the second and where the clipping occurs. The improved method (figures 6 and 7) does not suffer from this problem.

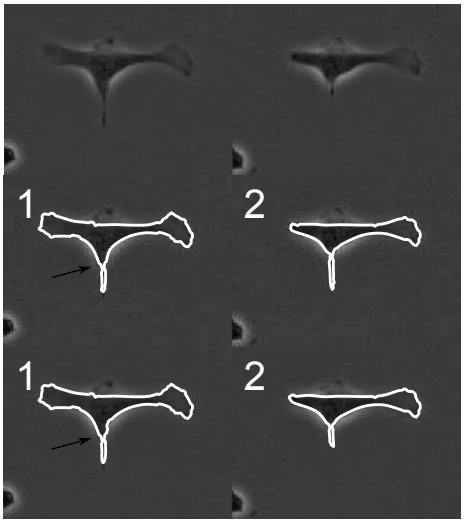

Fig. 6. Low-confidence removal allows better fitting into retracting protrusions. Middle: Self-intersection removal does not apply since retraction does not self-intersect. Bottom: Using low-confidence removal. Note that there are *no* self-intersections in these images, despite the appearance of overlap in the indicated area (black arrow). Rather, the overlap appears to occur because the contour have been thickened for display purposes.

IV. Performance

To quantify the performance of the method, the outlines that were produced were compared with manually-drawn contours. Let the points of the computer generated contour be $\hat{p}_i$, where i is an integer between 1 and n, and let the points of the manually-drawn contours be r_i, where i is an integer between 1 and m. The forward average Hausdorff distance is defined as:

$$d_f = \frac{1}{n}\sum_{i=1}^{n} d(\hat{p}_i, r) \tag{4}$$

Where $d(\hat{p}_i, r)$ is defined as the distance from the point $\hat{p}_i$ to contour r. In addition, the backward average Hausdorff distance is defined as:

$$d_b = \frac{1}{m}\sum_{i=1}^{m} d(r_i, p) \tag{5}$$

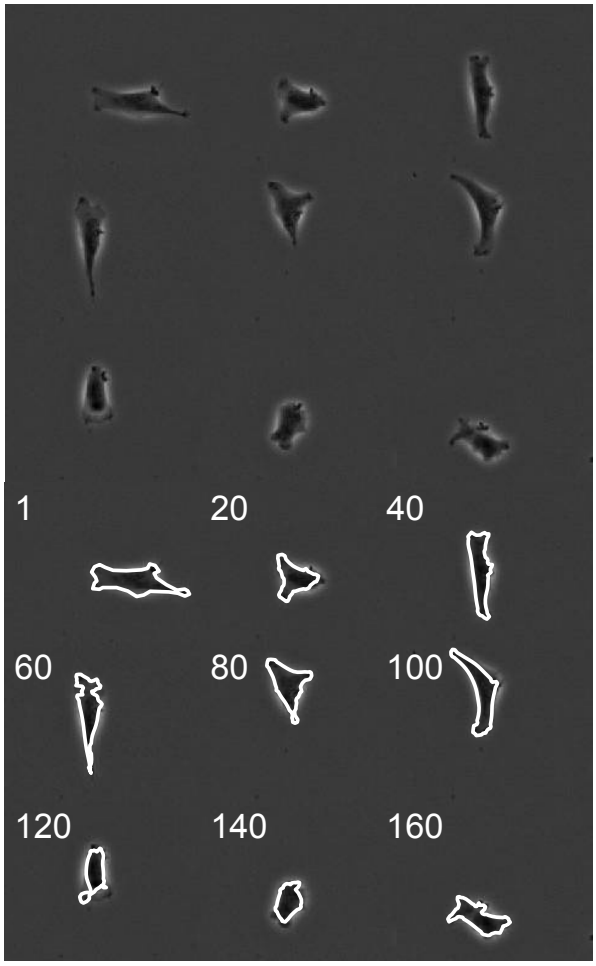

Fig. 7. Automatically-generated contours for an HMEC-1 cell moving in isolation. As can be seen, the high contrast for these cells enables a tight lock on the boundary for a large number of frames. Note that, as in Fig. 6, there are no self-intersections in these images.

For the fit on HMEC-1 cells, we observed that cell contrast is high enough that for each portion of the cell edge, the method either misses it entirely or is able to maintain a lock with sub-pixel accuracy (see Fig. 7). Therefore, the average distance would not be an effective indicator, since the distance at some points of the boundary would be very high and at others it would be very low. For the low-distance areas, any error would in our belief most likely be due to inconsistencies in manually-drawn lines (see Fig. 8). However, in the absence of any other objective metric, we use average Hausdorff distance as a baseline comparison.

V. Conclusions and Future Work

An active contour method was developed and applied to HMEC-1 cells, showing high performance and indicating the applicability of this active contour method to segmenting cells. The generated cell outlines and the average Hausdorff distance were shown for a single cell over 220 frames. 220 frames were chosen only since the cell in question is 'free' during this period and does not interact with other cells. We believe this method represents a powerful new tool for semi-

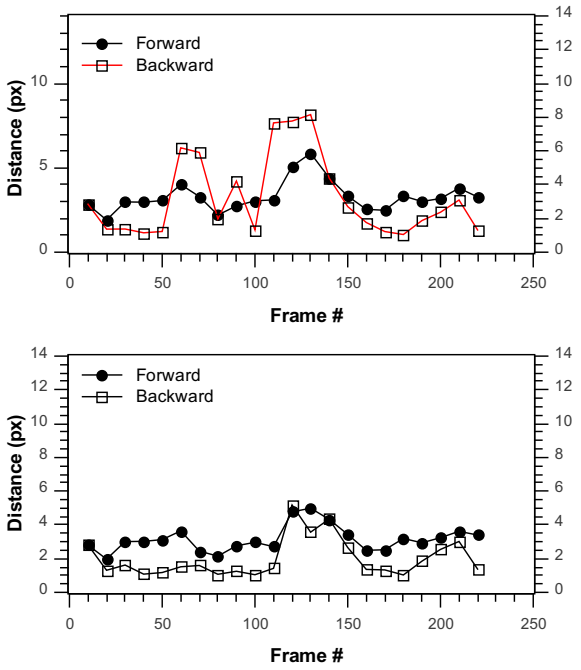

Fig. 8. Comparison of average contour distances between contour produced by our software and expert-drawn contour. Plot is for HMEC-1 cells. Top: with no low-confidence removal; bottom: with low-confidence removal. Even though the software is capable of 'recovering' into the right shape, low-confidence removal provides noticeable improvement in intermediate frames. As can be seen, the error rarely exceeds 6 pixels. In addition, the error is relatively consistent throughout the tracking period, indicating indicating that the lock on the cell is maintained.

automated tracking and analysis of cell movements, offering the opportunity of quantitative analyses on large data sets with minimized concern for tracking inaccuracies.

In addition, we have applied this method to low-contrast images of human hNT astrocytes and compared with the performance with previous active contour methods, such as those found in the popular ImageJ software. This will be subject of a future paper [11].

VI. Acknowledgements

We would like to thank the University of Auckland's Center for Brain Research for providing us access to cell cultures and live cell imaging facilities, and the Maurice and Phyllis Paykel Trust for their assistance in funding this work. We thank Associate Professor Larry Chamley of University of Auckland for access to the BioStation IM live cell imaging platform.

References

[1] J.C. Yarrow, Z.E. Perlman, N.J. Westwood, and T.J. Mitchison. A high-throughput cell migration assay using scratch wound healing, a comparison of image-based readout methods. *BMC Biotechnology*, 4, 2004.

[2] K. Li, E.D. Miller, M. Chen, T. Kanade, L.E. Weiss, and P.G. Campbell. Cell population tracking and lineage construction with spatiotemporal context. *Medical Image Analysis*, 12(5):546–566, 2008.

[3] PM Hauser and J. Errington. Characterization of cell cycle events during the onset of sporulation in bacillus subtilis. *Journal of bacteriology*, 177(14):3923, 1995.

[4] D.H. Rapoport, T. Becker, A.M. Mamlouk, S. Schicktanz, and C. Kruse. A novel validation algorithm allows for automated cell tracking and the extraction of biologically meaningful parameters. *PloS one*, 6(11):e27315, 2011.

[5] U. Ziegler, P. Groscurth, et al. Morphological features of cell death. *News in physiological sciences: an international journal of physiology produced jointly by the International Union of Physiological Sciences and the American Physiological Society*, 19:124, 2004.

[6] Michael Kass, Andrew Witkin, and Demetri Terzopoulos. Snakes: Active contour models. *International journal of computer vision*, 1(4):321–331, 1988.

[7] D. MacDonald, N. Kabani, D. Avis, and A.C. Evans. Automated 3-d extraction of inner and outer surfaces of cerebral cortex from mri. *NeuroImage*, 12(3):340–356, 2000.

[8] H. Shen, G. Nelson, S. Kennedy, D. Nelson, J. Johnson, D. Spiller, M.R.H. White, and D.B. Kell. Automatic tracking of biological cells and compartments using particle filters and active contours. *Chemometrics and Intelligent Laboratory Systems*, 82(1-2 SPEC. ISS):276–282, 2006.

[9] D. Dormann, T. Libotte, C.J. Weijer, and T. Bretschneider. Simultaneous quantification of cell motility and protein-membrane-association using active contours. *Cell motility and the cytoskeleton*, 52(4):221–230, 2002.

[10] K. Li, E.D. Miller, L.E. Weiss, P.G. Campbell, and T. Kanade. Online tracking of migrating and proliferating cells imaged with phase-contrast microscopy. In *Computer Vision and Pattern Recognition Workshop, 2006. CVPRW'06. Conference on*, pages 65–65. IEEE, 2006.

[11] A. Nejati, C.P. Unsworth, and E.S. Graham. High-precision active contours for tracking thin cell boundaries in phase contrast microscopy. *PLoS ONE*, under review, 2012.